Chlorophyll *a* Radical Ions: A Density Functional Study

Sebastian Sinnecker,[†,‡] Wolfram Koch,*[,‡,§] and Wolfgang Lubitz*[,†,||]

Max-Planck-Institut für Strahlenchemie, Postfach 101365, D-45413 Mülheim an der Ruhr, Germany, Institut für Chemie der Technischen Universität Berlin, Strasse des 17. Juni 135, D-10623 Berlin, Germany, and Max-Volmer-Laboratorium für Biophysikalische Chemie der Technischen Universität Berlin, Strasse des 17. Juni 135, D-10623 Berlin, Germany

Received: October 10, 2001; In Final Form: January 18, 2002

The chlorophyll *a* radical cation, Chl $a^{+\bullet}$, and the corresponding radical anion, Chl $a^{-\bullet}$, have been investigated applying density functional methods. Furthermore, the C^{10} epimer Chl *a*′ and O^1 Chl *a* enol radical cations have been studied, which have been proposed to play a role in photosystem I of oxygenic photosynthesis. Isotropic hyperfine coupling constants (hfcs) and related spin density distributions calculated at the B3LYP/EPR-II//BLYP/DZVP(D) level of theory are reported. For Chl $a^{+\bullet}$ and Chl $a^{-\bullet}$, good agreement is observed between calculated and experimental hfcs. Whereas no larger differences in the hfcs between Chl $a^{+\bullet}$ and (Chl a')$^{+\bullet}$ are predicted to occur, the enol forms of Chl $a^{+\bullet}$ give rise to significantly altered hyperfine coupling constants in comparison with the respective keto form. In addition to the chlorophyll systems, the epimer and O^1 enol of bacteriochlorophyll *a* have also been calculated. From a comparison with experimental data it is concluded that the enol forms do not occur in photosynthetic reaction centers.

1. Introduction

Chlorophyll and bacteriochlorophyll radical ions are created in the primary light reactions in photosynthetic reaction centers (RCs) of green plants and in bacteria.[1] The initial electron transfer in the RCs takes place between an excited specialized chlorophyll (Chl) or bacteriochlorophyll (BChl) species and another chlorophyll molecule before the electron is passed to other chlorophyll or pheophytin species and to quinone acceptors. Thereby the electron donor is transformed into a cation radical and all acceptors into anion radicals. *Electron paramagnetic resonance* (EPR) and related techniques such as *electron−nuclear double resonance* (ENDOR)[2,3] have been applied to elucidate the electronic structure of isolated chlorophyll radicals,[4−9] which is important for a functional understanding of the charge separation process in photosynthesis. Here the primary electron donor is of particular importance since it is located at the interface of exciton and electron transfer in the RC. In the photosynthetic purple bacteria this species has been found to be a BChl dimer.[10,11] In photosystem II of oxygenic photosynthesis the primary donor is probably a monomeric chlorophyll *a* species.[12,13] In photosystem I the donor is dimeric, but consists of Chl *a* and Chl *a*′, the C^{10} epimer of Chl *a* (see Scheme 1).[14] The exact geometry of the Chl *a* remains an open question, the existence of enol forms (ring V) cannot be excluded from the recent X-ray crystallographic structure at 2.5 Å resolution.[14,15] The structure of the primary donor (pigment P700) in photosystem I is shown in Figure 1.[14]

The respective cation radicals of the primary donors have been investigated by EPR and ENDOR spectroscopy to obtain information on the extent of electron spin delocalization in these species.[11,16,17] This is a key step in the elucidation of the electronic structure of the electron donors. To further understand these complex species, spectroscopic and theoretical investigations of the related monomeric (B)Chl-species are required.

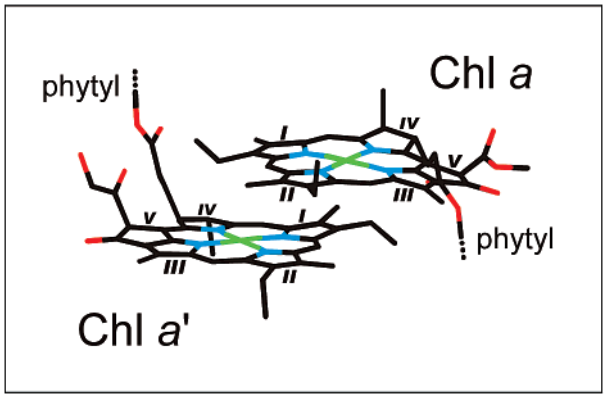

Figure 1. The structure of the chlorophyll dimer forming the primary electron donor P700 of photosystem (PS) I in oxygenic photosynthesis according to the X-ray structure analysis at 2.5 A resolution.[14] Note that the dimer is made up from a Chl *a* and a Chl *a*′ which differ in the position of the carbomethoxy group at the isocyclic ring V (see also Scheme 1). The planarity of the Chl *a* half appears to be distorted indicating a structural modification, in particular at ring V. The overlap of the two chlorophylls is at rings I and II. Color code: carbon (black), nitrogen (blue), oxygen (red), magnesium (green), protons not given. The phytyl chains are truncated.

Quantum chemical calculations can be used to study molecular structures as well as electric and magnetic properties of chlorophyll radicals, the results might be used, for example, as a theoretical basis for the assignment of measured isotropic hyperfine coupling constants. In this way, the semiempirical RHF-INDO/SP method applied to standard model systems without complete geometry optimization was a powerful tool for many years.[18] However, over the last years, methods based

* To whom correspondence should be addressed.
† Max-Planck-Institut für Strahlenchemie.
‡ Institut für Chemie der Technischen Universität.
§ Present address: Gesellschaft Deutscher Chemiker, Varrentrappstr. 40-42, D-60486 Frankfurt am Main, Germany.
|| Max-Volmer-Laboratorium für Biophysikalische Chemie der Technischen Universität.

10.1021/jp013758t CCC: $22.00
Published on Web 05/01/2002

SCHEME 1: Structure and Numbering of the Employed Chlorophyll Model Systems[a]

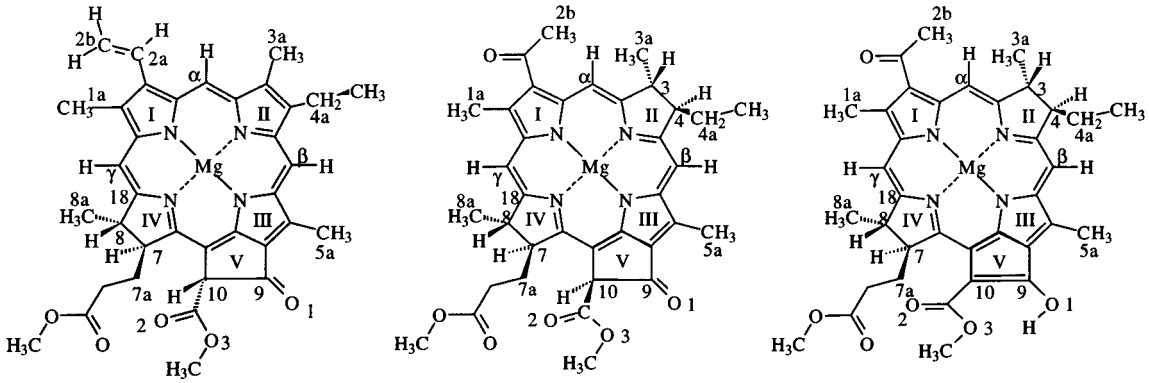

[a] The phytyl ester at pos. 7 was replaced by a methyl ester in all model systems. Chlorophyll *a* (left): The C^{10} epimer Chl *a*′ has the two substituents (H and the carbomethoxy group) at this position exchanged. The O^1 Chl *a* enol is the tautomer of Chl *a*, regarding the hydrogen migration between C^{10} and O^1. The corresponding derivatives of BChl *a*, namely, BChl *a*′ and BChl *a* enol, are also displayed (center and right).

on density functional theory have evolved as the computational strategy well suited for providing information of the magnetic properties of fairly large molecules, including complete geometry optimization. In recent work we have shown that calculated hfcs of the BChl *a* radical cation and anion at the B3LYP/EPR-II//BLYP/DZVP(D) level of density functional theory are in good agreement with the experimental data from ENDOR spectroscopy.[19] Similarly encouraging results were obtained by O'Malley in his density functional studies,[20−22] in which he concentrated on pheophytin anion radicals, lacking the central Mg ion. Chl *a* was investigated by O'Malley only by means of a small model system, disregarding almost all side chains.[23] This makes a direct comparison with experiments difficult. In addition to the calculation of magnetic resonance parameters, there is also growing theoretical interest in studying electronic excitations of chlorophylls.[24−26]

In the present work, isotropic hfcs of the chlorophyll *a* radical cation and anion (Scheme 1) are reported. Those are directly compared with experimentally determined coupling constants from ENDOR spectroscopy.[4−8] Furthermore, a comparison is performed with results from RHF-INDO/SP calculations. It should be noted, however, that the DFT/Fermi contact analysis is the proper method of obtaining hfcs and is applicable to a range of systems from organic radicals to transition metal complexes whereas the INDO method depends on parametrization to obtain hfcs from s-spin densities and only works well for specific types of radicals (see ref 18).

To assess the influence of various substituents and different conformers on the electronic structure of Chl $a^{+\bullet}$ and BChl $a^{+\bullet}$, calculations and experimental investigations on modified chlorophyll radicals are desirable. Here we focus on structural alterations of ring V of Chl *a* and BChl *a*, namely, the epimerical forms Chl *a*′ and BChl *a*′, and the O^1 enols (see Scheme 1). Both chlorophyll species, (Chl a')$^{+\bullet}$ and Chl $a^{+\bullet}$ enol have been suggested to play a role in the electron-transfer processes in earlier studies.[27,28]

2. Computational Details

To limit the calculations to a manageable size, the phytyl ester at position 7, as found in the native systems, has been replaced in all calculations by a methyl ester (see Scheme 1). All geometry optimizations were carried out using the gradient corrected density functional method BLYP[29−35] combined with the DZVP basis set to expand the Kohn−Sham orbitals.[36,37] In the case of the negatively charged Chl $a^{-\bullet}$, the basis set has been augmented by diffuse functions (labeled as DZVPD). More precisely, one diffuse function has been added for every valence shell, employing exponents equal to one-third of the smallest exponent in that particular shell.

For the determination of the EPR parameters, single point calculations on the optimized structures employing the three-parameter HF/DFT hybrid functional B3LYP have been performed.[35,38,39] In these calculations the EPR-II basis set was applied.[40] Since magnesium is not supported by this basis set, a TZVP basis set has been used for the metal.[36,37] All radical species were computed using the unrestricted Kohn−Sham formalism. Extensive studies on basis set dependence of hyperfine coupling constants at DFT level were already carried out by several authors.[40−43] In particular they have shown that the EPR and IGLO[44] functions perform well. Furthermore, our previous work on bacteriochlorophylls underlined the suitability of the EPR-II basis set, while the DZP basis set was only well suited for predicting ^{1}H coupling constants.[19]

The optimizations (Cartesian coordinates are available as Supporting Information) were performed employing the DGAUSS program package installed on a CRAY-J90 computer at ZIB Berlin,[45−47] allowing a maximum gradient of 9.0×10^{-4}. This program is particularly well-suited for multiprocessor applications and it avoids the time-consuming calculation of the four-center-two-electron coulomb integrals by expanding the density in an auxiliary basis set (in our work: A1 standard functions of the DGAUSS software). However, this approach and the DGAUSS program are restricted to pure density functional methods. Therefore, the B3LYP single point calculations have been carried out using the Gaussian 98 quantum chemical software,[48] installed on our own workstations.

For the sake of completeness, isotropic hyperfine coupling constants are also reported at the BLYP/DZVP(D) level of optimization. However, only the more sophisticated B3LYP/EPR-II//BLYP/DZVP(D) results will be discussed in the following sections.

3. Results and Discussion

The Chl *a* Radical Cation. For this molecule, experimental hfcs are available, but in contrast to the bacteriochlorophyll *a* cation radical, the uncertainties in the interpretation of the hydrogen coupling constants are somewhat larger.[4−7] The experimental assignments for the β-hydrogen atoms, methyl

TABLE 1: Experimental and Calculated Isotropic Hyperfine Coupling Constants (MHz) of the Chlorophyll *a* Radical Cation Chl $a^{+\bullet}$ (SP: Single Point Calculation Employing the Optimized Geometry)

	position	exptl[4]	RHF-INDO/SP[4]	BLYP DZVP	B3LYP EPR-II SP
β-H	7	+10.17[a]	+11.08	+13.50	+13.72
	8	+10.17[a]	+10.28	+13.60	+13.40
	10	−1.97	−1.50	−2.39	−4.68
CH_3	1a	+3.0[b]	+5.00	+1.70	+3.06
	5a	+7.12	+5.78	+7.28	+7.23
	3a	+3.0[b]	+4.18	+3.55	+4.31
	8a	−	−0.27	+0.02	−0.03
methine	α	+3.0	+4.40	+1.36	+4.90
	β	+3.0	+5.51	+2.00	+6.03
	δ	+0.57	+0.83	+0.01	+1.29
CH_2	7a		−0.60	−0.58	−0.75
	4a	+3.0	+1.74	+1.64	+1.31
vinyl-H	2a		+1.67	+0.37	+0.65
	2b	−2.20[c]	−0.36	−3.22	−2.47
^{14}N	I	−[d]	−1.47[c]	−0.58	−2.16
	II	−[d]	−2.29[c]	−1.31	−3.25
	III	−[d]	−1.38[c]	−0.95	−2.35
	IV	−[d]	−1.83[c]	−1.47	−2.77
Mg				−0.09	−0.51
$\langle S^2 \rangle$				0.756	0.782

[a] In ref 7, two slightly different hfcs have been measured (pos. 7: +10.30 MHz, pos. 8: +10.10 MHz.). [b] In a Chl *a* derivative (2-acetyl Chl $a^{+\bullet}$), two different hfcs were obtained showing that the assignment of this hfc to both positions 1a and 3a is correct (ref 4). [c] Value from ref 7. [d] No experimental isotropic ^{14}N coupling constants available for Chl $a^{+\bullet}$. Only anisotropic values from ESEEM experiments exist in the literature, see ref 49. The calculated values are in good agreement with the experimental ^{14}N hfcs of BChl $a^{+\bullet}$ (N^{I}: −2.24, N^{II}: −3.14, N^{III}: −2.32, N^{IV}: −2.89 MHz; ref 51).

groups, and methine ^1H nuclei could be confirmed, the smallest deviations between theory and experiment are obtained for the methyl group protons (Table 1 and Figure 2).

Experimental nitrogen and magnesium isotropic hyperfine coupling constants of Chl $a^{+\bullet}$ are to the best of our knowledge not available yet: only some anisotropic ^{15}N hfc tensor components have been measured by Käss et al.[49] From these experiments, negative isotropic ^{14}N hfcs between one and three MHz are expected for Chl $a^{+\bullet}$. The calculated ^{14}N coupling constants are in line with this finding. In addition, they are in good agreement with the ^{14}N hfcs calculated for a much smaller Chl $a^{+\bullet}$ model system (without alkyl or ester groups at positions 1, 3, 4, 5, 7, 8, and 10) employing the B3LYP/6-31G(d) level of theory (N^{I}: −2.1 MHz, N^{II}: −3.5 MHz, N^{III}: −2.1 MHz, N^{IV}: −2.4 MHz).[23] Furthermore, both computed sets of ^{14}N hfcs agree well with the nitrogen coupling constants of BChl $a^{+\bullet}$. Therefore, it can be concluded that the structural difference (Scheme 1) of BChl $a^{+\bullet}$ and Chl $a^{+\bullet}$ does not significantly affect the isotropic ^{14}N hyperfine coupling constants.

In comparison to the much faster RHF − INDO/SP calculations,[4] the B3LYP/EPR−II//BLYP/DZVP approach yielded improved ^1H hfcs for the methyl groups 1a and 5a. The semiempirical method gave results closer to the experiments in particular for the β-hydrogens at positions 7 and 8. In contrast, both techniques overestimate the methine hydrogen coupling constants. It has to be noted, however, that the assignment of the experimental hfcs to the methine hydrogens is not safe.

The singly occupied molecular orbital (SOMO) of Chl $a^{+\bullet}$ is shown as **1** in Figure 5. In addition, the spin density distribution of Chl $a^{+\bullet}$ is given as **2**. Note that the spin density distribution displays polarization effects in the molecule as a result of the exchange interaction between the unpaired α electron and other

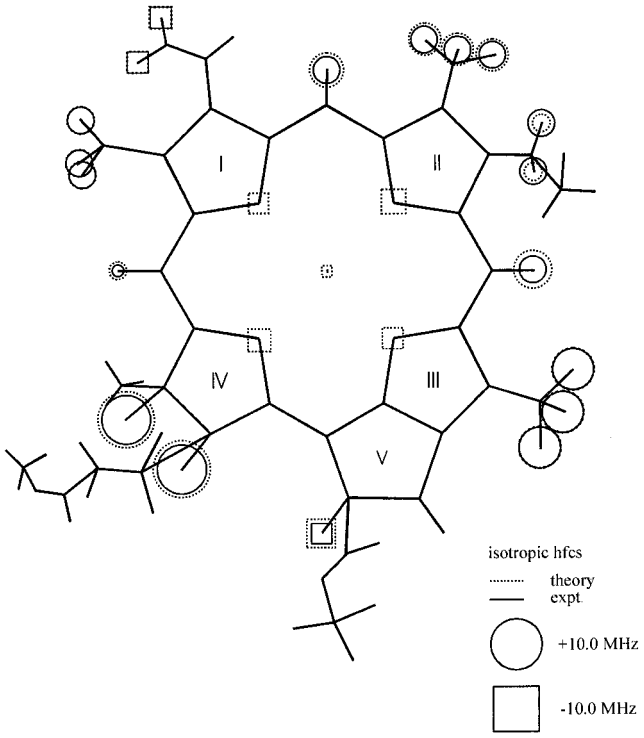

Figure 2. The Chl $a^{+\bullet}$ radical cation. Calculated (B3LYP/EPR−II//BLYP/DZVP) and measured isotropic hfcs, proportional to the areas of the circles and squares. ^1H hfcs ≤ 1 MHz are not displayed.

TABLE 2: Relative Energies of the Investigated Chlorophyll *a* Radicals

species	E_{rel}/kcal/mol (eV) BLYP/DZVP	E_{rel}/kcal/mol (eV) B3LYP/EPR-II SP
Chl *a*	0	0
Chl $a^{-\bullet}$	−[a]	−41.5 (−1.8)
Chl $a^{+\bullet}$	+139.6 (+6.0)	+141.9 (+6.1)
(Chl a')$^{+\bullet}$	+143.0 (+6.2)	+143.1 (+6.2)
Chl $a^{+\bullet}$ enol **A**	+135.8 (+5.9)	+139.3 (+6.0)
Chl $a^{+\bullet}$ enol **B**	+136.7 (+5.9)	+140.0 (+6.1)
Chl $a^{+\bullet}$ enol **C**	+149.8 (+6.5)	+151.3 (+6.6)

[a] Since the optimization of Chl $a^{-\bullet}$ was performed employing the DZVP basis augmented by diffuse functions, no data can be given for the stability of Chl $a^{-\bullet}$ at the DZVP level of theory.

electrons of same spin. While positive (α-excess) spin densities dominate, also negative values with an excess of β-spin density appear. For Chl $a^{+\bullet}$ negative values are found in particular at the positions of the nitrogen atoms and at the methine carbons.

In addition, the structure of the neutral singlet Chl *a* molecule has been optimized at the BLYP/DZVP level of theory. The optimization yielded a porphyrin structure with geometrical parameters, very similar to those obtained by Sundholm.[25] Mg−N bond distances differ for instance by less than 0.008 Å, somewhat larger differences are found for the N−C and C−C bond lengths of the heterocycle. In addition, we verified the very long C^9-C^{10} single bond in ring V with 1.620 Å (Sundholm: 1.594 Å, see Scheme 1).

Table 2 shows that the Chl $a^{+\bullet}$ radical ion is 139.6 kcal/mol less stable in the gas phase than the closed shell species. This BLYP/DZVP result is in good agreement with the relative energy obtained by the B3LYP/EPR-II//BLYP/DZVP single point calculation (+141.9 kcal/mol).

The Chl $a^{-\bullet}$ Radical Anion. The optimization of Chl $a^{-\bullet}$ resulted in a conformer similar to the cationic Chl $a^{+\bullet}$ and neutral Chl *a*. In all three cases, planar porphyrin structures with

TABLE 3: Experimental and Calculated Isotropic Hyperfine Coupling Constants (MHz) of the Chlorophyll *a* Radical Anion Chl $a^{-\bullet}$

	position	exptl[18,a]	RHF-INDO/SP[18]	BLYP DZVPD	B3LYP EPR-II SP
β-H	7	−0.30	−0.84	−0.23	−0.50
	8	+1.70	+1.93	+1.39	+1.29
	10	−1.53	−0.89	−0.10	−0.35
CH_3	1a	+5.43	+5.89	+6.30	+6.35
	5a	+10.58	+11.79	+11.02	+12.72
	3a	−1.53	−1.30	−0.81	−2.23
	8a	+0.54	+0.18	+0.57	+0.59
methine	α	−4.67	−7.86	−5.36	−5.92
	β	−11.68	−9.77	−9.11	−12.07
	δ	−4.37	−2.49	−3.85	−3.58
CH_2	7a	−	+0.05	+0.79	+0.19
	4a	−	−0.06	+0.30	+0.25
vinyl-H	2a	+1.45	+1.14	+0.09	+1.18
	$2b_1$	−2.32	−1.69	−3.72	−4.65
	$2b_2$	−2.48	−1.85	−3.86	−4.80
^{14}N	I	−2.03	−1.55	−0.71	−1.52
	II	+5.50	+7.36	+3.12	+4.20
	III	−0.55	−1.21	−0.48	−0.65
	IV	+4.44	+7.04	+4.04	+4.61
Mg			+0.64	+0.68	+0.89
$\langle S^2 \rangle$				0.753	0.772

[a] Experimental values from ref 8 but with the assignment of ref 18.

typical dihedral angels of ≤2° were obtained. However, a bending of ring IV was found, as indicated by the $C^7-C^8-C^{18}-N^{IV}$ dihedral angle. The values of 12.0° (Chl $a^{+\bullet}$), 12.5° (Chl *a*) and 12.2° (Chl $a^{-\bullet}$) demonstrate that this deviation from planarity is rather independent of the oxidation state of Chl *a*. The same behavior could be found for the vinyl group attached to ring I. This group is essentially located in the plane of the heterocycle in all three species, with deviations from exact planarity of about 3°. Since diffuse functions have been employed in the optimization of Chl $a^{-\bullet}$, the relative energy of this species in comparison to Chl *a* can be given only at the B3LYP/EPR−II//BLYP/DZVP level of theory (−41.5 kcal/mol, see Table 2).

The calculated hyperfine coupling constants are compiled in Table 3, a graphical illustration is displayed in Figure 3. A comparison with the experimental data (Table 3) shows reasonable agreement between theoretical and measured hfcs.[8] In comparison to the positively charged Chl $a^{+\bullet}$ the SOMO of Chl $a^{-\bullet}$ (**3** in Figure 5) shows increased values at C^9 and the neighboring oxygen O^1. The spin density map of Chl $a^{-\bullet}$ (**4** in Figure 5) shows less β-excess spin density in comparison to Chl $a^{+\bullet}$. The carbonyl group located at ring V exhibits more unpaired electron density than in Chl $a^{+\bullet}$. Such differences are not unexpected since both species differ by two electrons.

The (Chl *a*′)$^{+\bullet}$ Epimer. For Chl $a^{+\bullet}$ and its C^{10} epimer (Chl a')$^{+\bullet}$, very similar energies (Table 2) and hyperfine coupling constants (Table 4) were obtained. (Chl a')$^{+\bullet}$ is slightly less stable than Chl $a^{+\bullet}$ (1.2 kcal/mol = 0.05 eV at B3LYP/EPR-II//BLYP/DZVP). This is apparently due to an increased sterical hindrance between the alkyl substituents at positions 7 and 10 in the epimer leading to a slightly different geometry. All ^1H, ^{14}N, and ^{25}Mg hfcs are the same in both molecules to within ± 0.15 MHz, except for positions 7, 8, and 10, which show somewhat larger deviations.

The alterations in the hfcs, predicted theoretically for Chl $a^{+\bullet}$ and (Chl a')$^{+\bullet}$, are smaller than the deviations between theory and experiment obtained from the calculations on Chl $a^{+\bullet}$ and BChl $a^{+\bullet}$. Nevertheless, the trends given in the calculated data might be helpful for experimental investigations of (Chl a')$^{+\bullet}$.

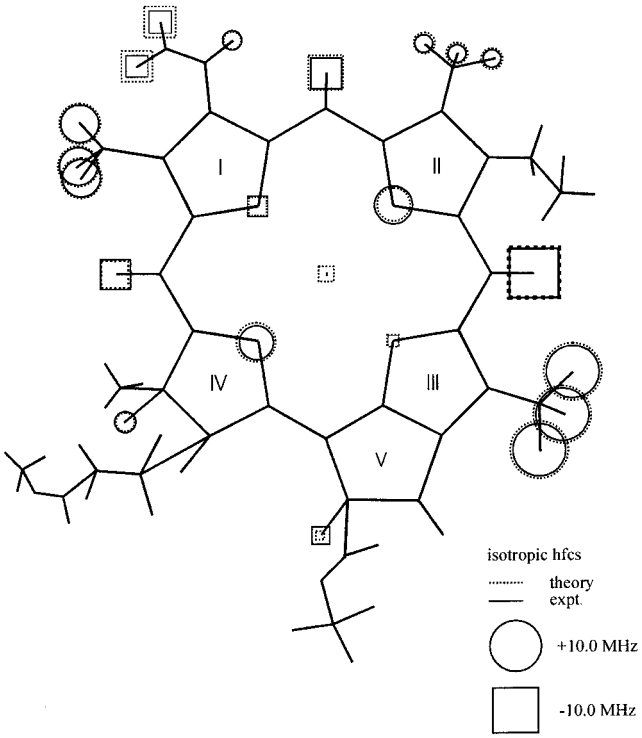

Figure 3. The Chl $a^{-\bullet}$ radical anion. Calculated (B3LYP/EPR-II//BLYP/DZVPD) and measured isotropic hfcs, proportional to the areas of the circles and squares. ^1H hfcs ≤ 1 MHz are not displayed.

TABLE 4: Isotropic Hyperfine Coupling Constants of the (Chl *a*′)$^{+\bullet}$ Epimer Radical Cation (MHz): For Comparison, the hfcs of Chl $a^{+\bullet}$ are Included

		Chl $a^{+\bullet}$	(Chl a')$^{+\bullet}$	
	position	B3LYP EPR-II SP	BLYP DZVP	B3LYP EPR-II SP
β-H	7	+13.72	+12.37	+12.56
	8	+13.40	+13.35	+13.07
	10	−4.68	−2.67	−5.01
CH_3	1a	+3.06	+1.70	+2.99
	5a	+7.23	+7.12	+7.36
	3a	+4.31	+3.55	+4.31
	8a	−0.03	−0.06	−0.11
methine	α	+4.90	+1.29	+4.77
	β	+6.03	+2.04	+6.12
	δ	+1.29	−0.05	+1.22
CH_2	7a	−0.75	−0.55	−0.75
	4a	+1.31	+1.47	+1.15
vinyl-H	2a	+0.65	+0.41	+0.70
	$2b_1$	−2.39	−3.08	−2.39
	$2b_2$	−2.54	−3.26	−2.55
^{14}N	I	−2.16	−0.54	−2.08
	II	−3.25	−1.30	−3.22
	III	−2.35	−1.02	−2.47
	IV	−2.77	−1.42	−2.71
Mg		−0.51	−0.09	−0.52
$\langle S^2 \rangle$		0.782	0.756	0.782

The Chl $a^{+\bullet}$ Enol. Geometry optimizations have been carried out considering four different isomers of this molecule (Scheme 2). While the calculation on the O^1 enol radical cation **D** as a starting structure resulted in structure **B**, all other isomers could be confirmed. The enol radical cation **C** is less favorable in energy than the corresponding isomers **A** and **B** owing to the missing hydrogen bond (see Table 2). Structures **A** and **B** are not only of similar energy, both radicals are also somewhat more stable than Chl $a^{+\bullet}$ in the gas-phase calculations. A higher stability of the respective enol radical cation is not unusual, it

TABLE 5: Isotropic Hyperfine Coupling Constants of the Chl $a^{+\bullet}$ Enol Radical Cations A, B and C (see Scheme 2) in MHz: For Comparison, the hfcs of Chl $a^{+\bullet}$ are also Listed

		Chl $a^{+\bullet}$	Chl $a^{+\bullet}$ enol **A**		Chl $a^{+\bullet}$ enol **B**		Chl $a^{+\bullet}$ enol **C**	
	position	B3LYP EPR-II SP	BLYP DZVP	B3LYP EPR-II SP	BLYP DZVP	B3LYP EPR-II SP	BLYP DZVP	B3LYP EPR-II SP
β-H	7	+13.72	−1.36	−3.36	−1.10	−3.07	−1.20	−3.08
	8	+13.40	−0.26	−1.78	−0.60	−2.51	−0.37	−1.75
	10	−4.68						
OH	O[1]		−1.70	−1.49	−1.93	−1.84	−3.10	−2.90
CH_3	1a	+3.06	+2.14	+3.63	+3.31	+3.07	+2.12	+3.54
	5a	+7.23	−1.08	−1.79	−1.06	−1.53	−1.35	−2.97
	3a	+4.31	+4.12	+5.83	+3.86	+5.34	+4.21	+5.60
	8a	−0.03	+0.50	+0.51	+0.48	+0.48	+0.44	+0.46
methine	α	+4.90	−4.60	−3.82	−4.48	−4.16	−2.90	−1.58
	β	+6.03	−2.01	+1.17	−2.07	+0.62	−0.15	+3.41
	δ	+1.29	−8.34	−11.03	−8.07	−10.87	−7.09	−9.17
CH_2	7a	−0.75	+0.35	+0.45	+0.23	+0.37	+0.16	+0.30
	4a	+1.31	−0.41	−1.14	−0.42	−1.16	−0.32	−0.90
vinyl-H	2a	+0.65	−0.30	−1.20	−0.28	−1.11	−0.25	−0.98
	$2b_1$	−2.39	+0.61	+1.87	+0.59	+1.82	+0.54	+1.66
	$2b_2$	−2.54	+0.63	+1.97	+0.61	+1.92	+0.57	+1.76
^{14}N	I	−2.16	+1.09	+1.31	+1.05	+1.41	+0.77	+0.83
	II	−3.25	−0.20	−1.27	−0.16	−1.00	−0.59	−1.76
	III	−2.35	+1.70	+0.44	+1.80	+0.72	+1.88	+0.63
	IV	−2.77	+3.34	+4.53	+3.50	+4.84	+3.06	+4.11
Mg		−0.51	+0.63	+0.77	+0.63	+0.83	+0.57	+0.67
$\langle S^2 \rangle$		0.782	0.755	0.783	0.754	0.782	0.754	0.782

SCHEME 2: Ring V Geometry of the Four Investigated Chl *a* Enols[a]

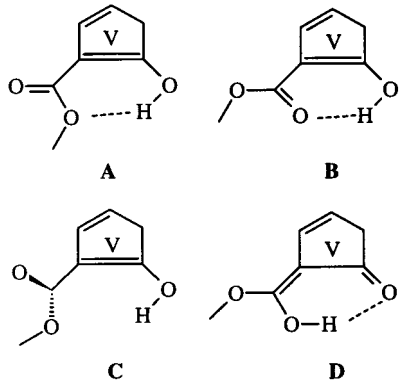

[a] No stationary point could be found at the BLYP/DZVP level of theory for geometry **D**.

was also found by Schwarz and co-workers who investigated substituent effects on ionized tautomers of ethanal.[50]

The SOMO's and spin densities of the Chl $a^{+\bullet}$ enol radical cations are distinctly different from Chl $a^{+\bullet}$ (see Figure 5). In consequence, also the hyperfine coupling constants differ clearly from those of the Chl $a^{+\bullet}$ parent molecule (Table 5 and Figure 4): (i) While strong β-hydrogen coupling constants at position 7 and 8 are found for Chl $a^{+\bullet}$, rather small and even negative hfcs are obtained for the enol radical cations. (ii) Among the CH_3 coupling constants only 5a shows a strong change in magnitude in the enol forms. (iii) All methine hfcs are changed, the largest hyperfine coupling constant is now that of the δ-methine ^1H nucleus. (iv) Only one small negative ^{14}N hfc is predicted to occur in the enols (for N^{II}), while positive coupling constants are obtained for N^{I}, N^{III}, and N^{IV}, that of N^{IV} is particularly large. In contrast, Chl $a^{+\bullet}$ is expected to show four negative ^{14}N hfcs.

Wasielewski and co-worker investigated chlorophyll *a* enol indirectly employing a silyl enol ether and the 9-desoxo-9,10-dehydro Chl $a^{+\bullet}$ radical cation.[27] The latter alkene was used in EPR investigations. The authors concluded from a comparison

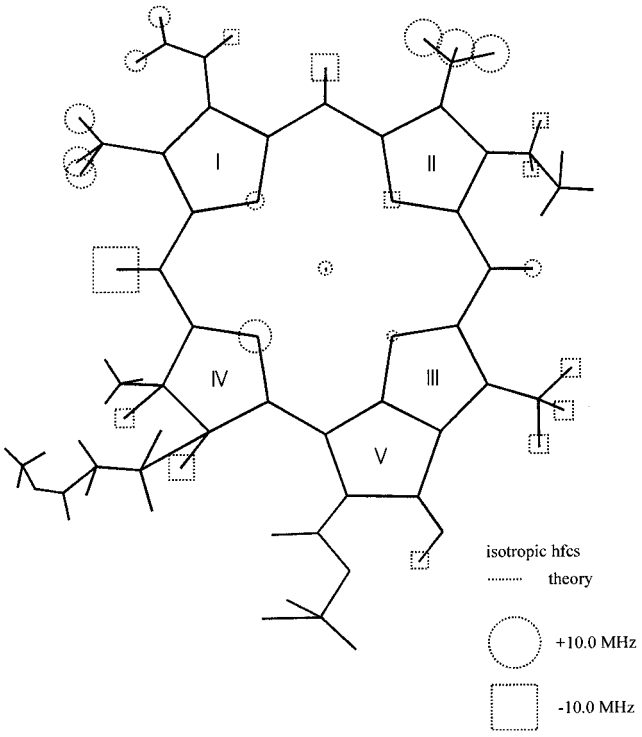

Figure 4. The Chl $a^{+\bullet}$ enol radical cation (geometry **A**). Calculated (B3LYP/EPR-II//BLYP/DZVP) and measured isotropic hfcs, proportional to the areas of the circles and squares. ^1H hfcs ≤ 1 MHz are not displayed.

of the measured ESR line width of 9-desoxo-9,10-dehydro Chl $a^{+\bullet}$ and several other mono- and dimeric chlorophyll radicals, that the spin distribution of an enol radical cation should differ significantly from that of Chl $a^{+\bullet}$. Furthermore, rather small spin density values were predicted to occur for the nitrogen nuclei and for carbon atoms in α position to methyl groups and hydrogens. In an ENDOR investigation of 9-desoxo-9,10-dehydro Chl $a^{+\bullet}$ only one characteristic hyperfine coupling constant of +3.5 MHz could be obtained, it was assigned to the methyl group at position 3a. Our calculations gave coupling

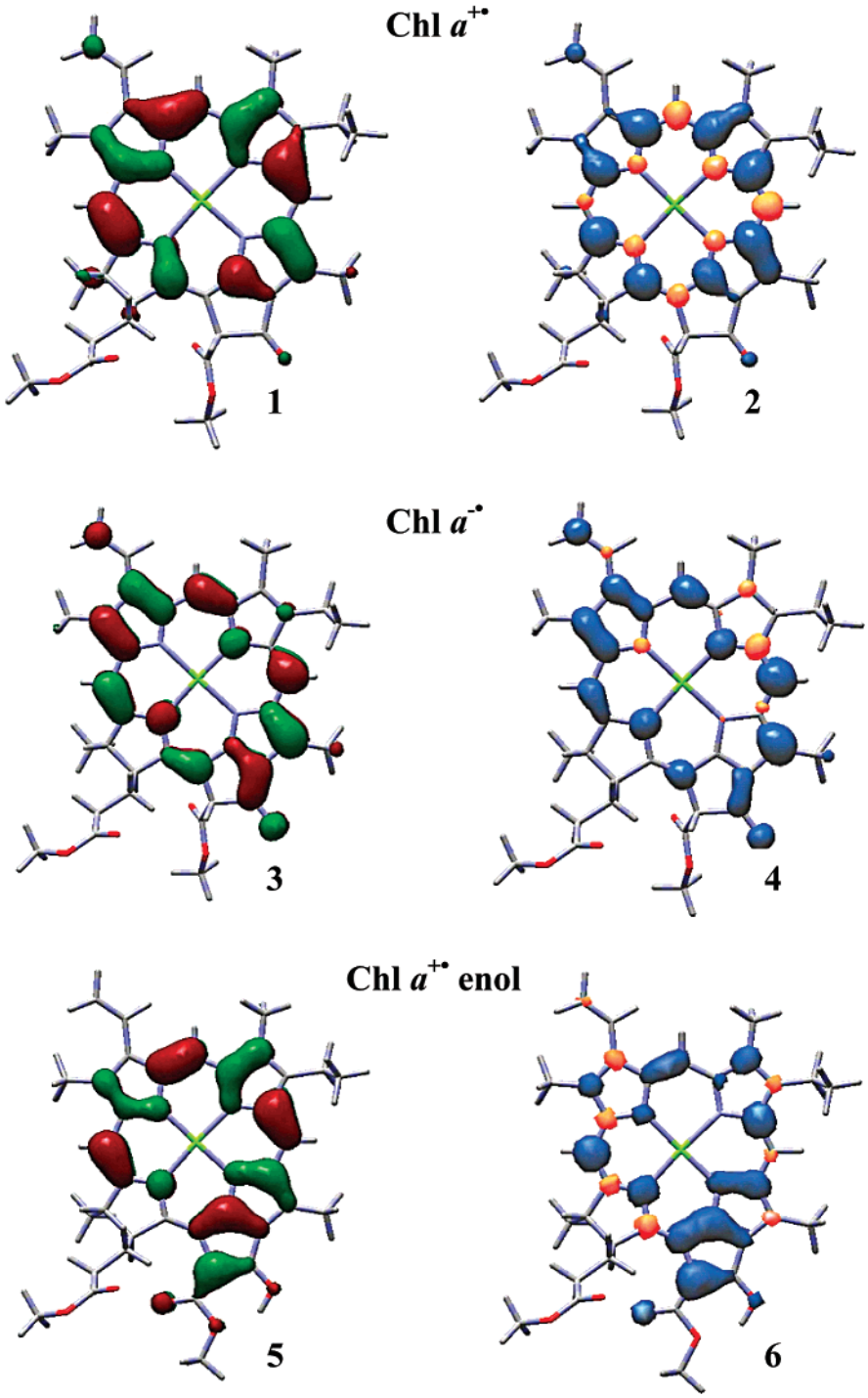

Figure 5. The singly occupied molecular orbitals (SOMO) of Chl $a^{+\bullet}$ (**1**), Chl $a^{-\bullet}$ (**3**) and Chl $a^{+\bullet}$ enol **A** (**5**). Spin density distributions of Chl $a^{+\bullet}$ (**2**), Chl $a^{-\bullet}$ (**4**), and Chl $a^{+\bullet}$ enol (**6**). Displayed are Gauss View figures employing the B3LYP/EPR-II//BLYP/DZVP(D) wave functions. Orbitals and spin densities are plotted using isodensity values of 0.03 and 0.002, respectively. Note that the spin densities have positive (blue) and negative (orange) signs due to spin polarization (**2**, **4** and **6**).

constants of +5.3 to +5.8 MHz for that group (Table 5). In contrast, the large coupling constants of −9 to −11 MHz, calculated for the δ-methine hydrogen, could not be found in the experiments which might be due to the high anisotropy of this ^{1}H hfc. However, one has to keep in mind that different systems have been studied. While the alkene without hydroxyl group at ring V has been investigated in the experiment, O[1] enol radicals have been studied in our calculations.

The Bacteriochlorophyll Derivatives (BChl *a*′)$^{+\bullet}$ and BChl *a*$^{+\bullet}$ Enol. Epimer or enol forms of the bacteriochlorophylls have not been reported to occur in bacterial photosynthesis. Hence, the theoretical results are only presented briefly.

The calculated ^{1}H, ^{14}N and ^{25}Mg isotropic hyperfine coupling constants of (BChl *a*′)$^{+\bullet}$ are compiled in Table 6. They are compared with the experimental results[51,52] and the computed hfcs of BChl *a*$^{+\bullet}$.[19] As in the case of Chl *a*$^{+\bullet}$ and (Chl *a*′)$^{+\bullet}$, the calculated hfcs of (BChl *a*′)$^{+\bullet}$ and BChl *a*$^{+\bullet}$ are very similar. The largest absolute deviations were also found for the β-hydrogens.

To save computational resources, only the BChl *a*$^{+\bullet}$ enol radical cation corresponding to form **A** (see Scheme 2) has been investigated. Significant differences in the coupling constants of BChl *a*$^{+\bullet}$ and BChl *a*$^{+\bullet}$ enol are obtained (Table 6) similar to those of the chlorophyll system.

TABLE 6: Isotropic Hyperfine Coupling Constants of the (BChl *a*′)$^{+\bullet}$ Epimer Radical Cation and the BChl *a*$^{+\bullet}$ Enol Radical Cation (MHz): For Comparison, the hfcs of BChl *a*$^{+\bullet}$ are Included

		BChl *a*$^{+\bullet}$		(BChl *a*′)$^{+\bullet}$		BChl *a*$^{+\bullet}$ enol	
	position	exptl[43]	B3LYP EPR-II SP[19]	BLYP DZVP	B3LYP EPR-II SP	BLYP DZVP	B3LYP EPR-II SP
β-H	3	+13.47	+12.25	+13.05	+13.71	+4.40	+6.47
	4	+16.35	+14.84	+15.55	+16.80	+15.11	+18.47
	7	+13.11	+14.40	+12.19	+12.89	+0.25	+1.05
	8	+11.76	+13.21	+11.97	+12.58	+2.18	+3.46
CH_3	1a	+4.93	+4.55	+4.88	+5.29	+2.92	+4.57
	5a	+9.62	+9.99	+9.14	+10.18	+0.52	+0.72
methine	α	+2.35	+4.11	+1.67	+4.24	+0.19	+3.38
	β	+1.30	+2.93	+0.30	+2.78	−3.21	+0.55
	δ	+1.30	+3.39	+0.97	+3.32	−3.71	−3.49
other	7a	−0.51	−0.82	−0.50	−0.77	+0.06	−0.05
	8a	−0.15	−0.16	−0.09	−0.20	+0.21	+0.23
	2b	−0.15	+0.19	+0.12	−0.01	−0.05	−0.04
	3a	−0.36	−0.27	−0.16	−0.28	−0.15	−0.36
	4a	−0.36	−0.17	−0.04	−0.19	+0.29	+0.04
	10	−1.64	−5.14	−2.66	−5.67		
OH	O^1					−0.72	−0.11
^{14}N	ring I	−2.24	−2.52	−1.23	−2.56	−0.14	−0.94
	ring II	−3.14	−3.58	−1.59	−3.58	−0.24	−2.70
	ring III	−2.32	−2.67	−1.22	−2.63	−0.03	−2.12
	ring IV	−2.89	−3.74	−1.60	−3.61	+1.07	+0.52
^{25}Mg		−0.30	−0.69	−0.20	−0.70	+0.23	−0.10
$\langle S^2 \rangle$			0.782	0.757	0.782	0.754	0.775

4. Summary and Conclusion

The calculated isotropic hyperfine coupling constants (B3LYP/EPR−II//BLYP/DZVP(D)) of the chlorophyll *a* radical cation and anion are in good agreement with the experimental results, especially for the methyl groups.

A Chl *a*′ has been found to constitute one half of the chlorophyll dimer of the primary donor P700 in photosystem I of oxygenic photosynthesis. Thus, a theoretical investigation of the cation radicals of Chl *a* and Chl *a*′, including complete structural optimizations, was appropriate. It was found, that the coupling constants of (Chl *a*′)$^{+\bullet}$ are barely distinguishable from those of Chl *a*$^{+\bullet}$. Noticeable differences are calculated only for the large coupling constants of the β-hydrogens which is mainly caused by a somewhat different geometry of the hydrogenated rings. Hence, a distinction between Chl *a*$^{+\bullet}$ and the corresponding epimer radical cation applying electron spin resonance methods will be rather difficult. This is particularly true when these species are embedded in a protein environment where pigment−protein interaction can easily change geometry and electronic structure. Similar small differences in the hfcs are obtained for BChl *a*$^{+\bullet}$ and its epimer.

The enol forms of Chl *a*$^{+\bullet}$ and BChl *a*$^{+\bullet}$ are characterized by strongly altered hfcs in comparison with Chl *a*$^{+\bullet}$ and BChl *a*$^{+\bullet}$, respectively. This is due to the different π electron delocalization in the enols for which the electronic and geometrical structure of ring V is significantly changed (Scheme 2). The calculations show that the SOMO for all enol forms is quite different from that of the keto form. It has been proposed by Wasielewski et al.[27] that enolic forms of Chl *a* could occur in the primary donor P700 of photosystem I of plant photosynthesis. In particular, the low oxidation potential of P700 (440 mV) as compared to that of monomeric Chl *a* in solution (700−1000 mV)[53] could arise from such an enolization process. However, the spin density distributions of the enolic forms calculated here are very different from those observed in ENDOR experiments performed on P700$^{+\bullet}$.[16] For example, the two β-proton hfcs are clearly the largest hfcs in P700$^{+\bullet}$. Furthermore, the CH_3 group at position 5a could be assigned and shows appreciable coupling strength.[16] This is different in the calculation performed on the enol radical cation. On the bases of our calculations, an enolic form of Chl *a* is therefore unlikely to contribute to P700. However, an altered geometry of ring V has been reported for the Chl *a* half of P700 in the recent X-ray crystallographic structure.[14] This could be responsible for some of the observed peculiarities of this species in vivo. This was proposed already by O'Malley and Babcock.[54] They found a monomeric spin density distribution of P700$^{+\bullet}$, although the molecular structure is dimeric.[14−16,55]

In a next step, experimental investigations of the respective chlorophyll derivatives (*a*′ and *a* enol) or related model systems would be desirable. A reliable calculation of redox potentials might be helpful for a further understanding of the electron-transfer processes. The investigation of Chl *a*$^{+\bullet}$, (Chl *a*′)$^{+\bullet}$ and the corresponding bacteriochlorophyll *a* radical cations provides a reference for future examinations of chlorophyll dimers. Such calculations are under way in our laboratory. However, density functional studies on such large systems are still a computational challenge.

Acknowledgment. Dr. M. Plato (FU Berlin) is acknowledged for providing the RHF-INDO/SP program. We thank Drs. N. Krauss, P. Jordan (FU Berlin), and P. Fromme (TU Berlin) for providing details on the structure of the primary donor in photosystem I. We thank the Konrad−Zuse−Zentrum, Berlin, for generously providing computer time and the DGAUSS software. This work has been supported by Deutsche Forschungsgemeinschaft (Sfb 498, Teilprojekt C5) and EU (FMRX-CT98-0214). Furthermore, support by Fonds der Chemischen Industrie to W.L. and W.K. is gratefully acknowledged.

Supporting Information Available: Optimized cartesian coordinates for all investigated radicals. This material is available free of charge via the Internet at http://pubs.acs.org.

References and Notes

(1) Hoff, A. J.; Deisenhofer, J. *Phys. Rep.* **1997**, *287*, 1.

(2) Weil, J. A.; Bolton, J. R.; Wertz, J. E. *Electron Paramagnetic Resonance−Elementary Theory and Practical Applications*; Wiley: New York, 1994.

(3) Kurreck, H.; Kirste, B.; Lubitz, W. *Electron Nuclear Double Resonance Spectroscopy of Radicals in Solution;* VCH: Weinheim, 1988.
(4) Käss, H.; Lubitz, W.; Hartwig, G.; Scheer, H.; Noy, D.; Scherz, A. *Spectrochim. Acta A* **1998**, *54*, 1141.
(5) Käss, H.; Rautter, J.; Zweygart, W.; Struck, A.; Scheer, H.; Lubitz, W. *J. Phys. Chem*. **1994**, *98*, 354.
(6) Scheer, H.; Katz, J. J.; Norris, J. R. *J. Am. Chem. Soc*. **1977**, *99*, 1372.
(7) Huber, M.; Lendzian, F.; Lubitz, W.; Tränkle, E.; Möbius, K.; Wasielewski, M. R. *Chem. Phys. Lett*. **1986**, *132*, 467.
(8) Hoff, A. J.; Lendzian, F.; Möbius, K.; Lubitz, W. *Chem. Phys. Lett*. **1982**, *85*, 3.
(9) Forman, A.; Davis, M. S.; Fujita, I.; Hansson, L. K.; Smith, K. M.; Fajer, J. *Isr. J. Chem*. **1981**, *21*, 265.
(10) Lancaster, C. R. D.; Ermler, U.; Michel, H. In *The Structure of Photosynthetic Reaction Centers from Purple Bacteria as Revealed by X-ray Crystallography*; Blankenship, R. E., Madigan, M. T., Bauer, C. E., Eds.; Kluwer Academic Publishers: Dordrecht, 1995; Vol. 2, pp 503−526.
(11) Lendzian, F.; Huber, M.; Isaacson, R. A.; Endeward, B.; Plato, M.; Bönigk, B.; Möbius, K.; Lubitz W.; Feher, G. *Biochim. Biophys. Acta* **1993**, *1183*, 139.
(12) Zouni, A.; Witt, H. T.; Kern, J.; Fromme, P.; Krauss, N.; Saenger, W.; Orth, P. *Nature* **2001**, *409*, 739.
(13) Lubitz, W.; Lendzian, F.; Bittl, R. *Acc. Chem. Res*. **2001**. In press.
(14) Jordan, P.; Fromme, P.; Witt, H. T.; Klukas, O.; Saenger, W.; Krauss, N. *Nature* **2001**, *411*, 909. See also Brookhaven data bank under accession number 1JB0.
(15) Webber, A. N.; Lubitz, W. *Biochim. Biophys. Acta* **2001**, *1507*, 61.
(16) Käss, H.; Fromme, P.; Witt, H. T.; Lubitz, W. *J. Phys. Chem. B* **2001**, *105*, 1225.
(17) Rigby, S. E. J.; Nugent, J. H. A.; O'Malley, P. J. *Biochemistry* **1994**, *33*, 10043.
(18) Plato, M.; Möbius, K.; Lubitz, W. In *Chlorophylls*; Scheer, H., Ed.; CRC Press: Boca Raton, 1991; pp 1015−1046.
(19) Sinnecker, S.; Koch, W.; Lubitz, W. *Phys. Chem. Chem. Phys*. **2000**, *2*, 4772.
(20) O'Malley, P. J. *J. Phys. Chem. B* **2000**, *104*, 2176.
(21) O'Malley, P. J. *J. Am. Chem. Soc*. **1999**, *121*, 3185.
(22) O'Malley, P. J. *J. Comput. Chem*. **1999**, *20*, 1292.
(23) O'Malley, P. J. *J. Am. Chem. Soc*. **2000**, *122*, 7798.
(24) Parusel, A. B. J.; Grimme, S. *J. Phys. Chem. B* **2000**, *104*, 5395.
(25) Sundholm, D. *Chem. Phys. Lett*. **2000**, *317*, 545.
(26) Sundholm, D. *Chem. Phys. Lett*. **1999**, *302*, 480.
(27) Wasielewski, M. R.; Norris, J. R.; Shipman, L. L.; Lin, C.-P.; Svec, W. A. *Proc. Natl. Acad. Sci. U.S.A.* **1981**, *78*, 2957.
(28) Kobayashi, M.; Watanabe, T.; Nakazato, M.; Ikegami, I.; Hiyama, T.; Matsunaga, T.; Murata, N. *Biochim. Biophys. Acta* **1988**, *81*, 936.
(29) Koch, W.; Holthausen, M. C. *A Chemist's Guide to Density Functional Theory*; Wiley-VCH: Weinheim, 2000.
(30) Hohenberg, P.; Kohn, W. *Phys. Rev. B* **1964**, *136*, 864.
(31) Kohn, W.; Sham, L. J. *Phys. Rev. A* **1965**, *140*, 1133.
(32) Parr, R. G.; Yang, W. *Density-Functional Theory of Atoms and Molecules*; Oxford University Press: Oxford, 1989.
(33) Malkin, V.; Malkina, O. L.; Eriksson, L. A.; Salahub, D. R. In *Modern Density Functional Theory; A Tool for Chemistry. Theoretical and Computational Chemistry;* Seminario, J. M.; Politzer, P., Eds.; Elsevier: Amsterdam, 1995; Vol. 2.
(34) Becke, A. D. *Phys. Rev. B* **1988**, *38*, 3098.
(35) Lee, C.; Yang, W.; Parr, R. G. *Phys. Rev. B* **1988**, *37*, 785.
(36) Godbout, N.; Salahub, D. R.; Andzelm, J.; Wimmer, E. *Can. J. Chem*. **1992**, *70*, 560.
(37) Sosa, C.; Andzelm, J.; Elkin, B. C.; Wimmer, E. *J. Phys. Chem*. **1992**, *96*, 6630.
(38) Becke, A. D. *J. Chem. Phys*. **1993**, *98*, 5648.
(39) Stephens, P. J.; Devlin, J. F.; Chabalowski, C. F.; Frisch, M. J. *J. Phys. Chem*. **1994**, *98*, 11623.
(40) Barone, V. In *Recent Advances in Density Functional Methods*; Chong, D. P., Ed.; World Scientific Publishing Co.: Singapore, 1996.
(41) Engels, B.; Eriksson, L. A.; Lunell, S. *Adv. Quantum. Chem*. **1996** *27*, 297.
(42) Munzarová, M.; Kaupp, M. *J. Phys. Chem. A*, **1999** *103*, 9966.
(43) Eriksson, L. A. *J. Chem. Phys*. **1994** *100*, 5066.
(44) Kutzelnigg, W.; Fleischer, U.; Schindler, M. In *NMR−Basic Principles and Progress*, Springer-Verlag: Heidelberg, 1990; Vol. 23, p 165.
(45) Andzelm, J. In *Density Functional Methods in Chemistry*; Labanowski, J., Andzelm, J., Eds.; Springer-Verlag: New York, 1991; p 155.
(46) Andzelm, J.; Wimmer, E. *J. Chem. Phys*. **1992**, *96*, 1280.
(47) *ACS Symposium Series 394*; Andzelm, J., Wimmer, E., Salahub, D. R., Zerner, M. C., Eds.; American Chemical Society: Washington, DC, 1989; p 228.
(48) Frisch, M. J.; Trucks, G. W.; Schlegel, H. B.; Scuseria, G. E.; Robb, M. A.; Cheeseman, J. R.; Zakrzewski, V. G.; Montgomery, J. A., Jr.; Stratmann, R. E.; Burant, J. C.; Dapprich, S.; Millam, J. M.; Daniels, A. D.; Kudin, K. N.; Strain, M. C.; Farkas, O.; Tomasi, J.; Barone, V.; Cossi, M.; Cammi, R.; Mennucci, B.; Pomelli, C.; Adamo, C.; Clifford, S.; Ochterski, J.; Petersson, G. A.; Ayala, P. Y.; Cui, Q.; Morokuma, K.; Malick, D. K.; Rabuck, A. D.; Raghavachari, K.; Foresman, J. B.; Cioslowski, J.; Ortiz, J. V.; Stefanov, B. B.; Liu, G.; Liashenko, A.; Piskorz, P.; Komaromi, I.; Gomperts, R.; Martin, R. L.; Fox, D. J.; Keith, T.; Al-Laham, M. A.; Peng, C. Y.; Nanayakkara, A.; Gonzalez, C.; Challacombe, M.; Gill, P. M. W.; Johnson, B.; Chen, W.; Wong, M. W.; Andres, J. L.; Gonzalez, C.; Head-Gordon, M.; Replogle, E. S.; Pople, J. A. *Gaussian 98*; Gaussian, Inc.: Pittsburgh, PA, 1998.
(49) Käss, H.; Bittersmann-Weidlich, E.; Andréasson, L.-E.; Bönigk, B.; Lubitz, W. *Chem. Phys*. **1995**, *194*, 419.
(50) Heinrich, N.; Frenking, G.; Koch, W.; Schwarz, H. *J. Am. Chem. Soc*. **1986**, *108*, 593.
(51) Lubitz, W.; Lendzian, F.; Plato, M.; Scheer, H.; Möbius, K. *Appl. Magn. Reson*. **1997**, *13*, 531.
(52) Lendzian, F.; Möbius, K.; Plato, M.; Smith, U. H.; Thurnauer, M. C.; Lubitz, W. *Chem. Phys. Lett*. **1984**, *111*, 583.
(53) Watanabe, T.; Kobayashi, M. In *Chlorophylls*; Scheer, H., Ed.; CRC Press: Boca Raton, 1991; p 287.
(54) O'Malley, P. J.; Babcock, G. T. *Proc. Natl. Acad. Sci. U.S.A.*, **1984**, *81*, 1098.
(55) Plato, M.; Krauss, N.; Fromme, P.; Lubitz, W. **2002**, submitted.